Wind and Structures, *Vol. 17, No. 6 (2013) 609-627*
DOI:http://dx.doi.org/10.12989/was.2013.17.6.609

Full-scale measurements of wind effects and modal parameter identification of Yingxian wooden tower

Bo Chen*[1], Qingshan Yang[1], Ke Wang[1] and Linan Wang[2]

[1]*School of Civil Engineering, Beijing Jiaotong University, Haidian District, Beijing, China*
[2]*Chinese Academy of Cultural Heritage, Chaoyang District, Beijing, China*

(Received October 22, 2012, Revised April 4, 2013, Accepted July 11, 2013)

Abstract. The Yingxian wooden tower in China is currently the tallest wooden tower in the world. It was built in 1056 AD and is 65.86 m high. Field measurements of wind speed and wind-induced response of this tower are conducted. The wind characteristics, including the average wind speed, wind direction, turbulence intensity, gust factor, turbulence integral length scale and velocity spectrum are investigated. The power spectral density and the root-mean-square wind-induced acceleration are analyzed. The structural modal parameters of this tower are identified with two different methods, including the Empirical Mode Decomposition (EMD) combined with the Random Decrement Technique (RDT) and Hilbert transform technique, and the stochastic subspace identification (SSI) method. Results show that strong wind is coming predominantly from the West-South of the tower which is in the same direction as the inclination of the structure. The Von Karman spectrum can describe the spectrum of wind speed well. Wind-induced torsional vibration obviously occurs in this tower. The natural frequencies identified by EMD, RDT and Hilbert Transform are close to those identified by SSI method , but there is obvious difference between the identified damping ratios for the first two modes.

Keywords: wooden tower; full-scale measurement; wind speed; wind-induced response; modal parameter

1. Introduction

The Yingxian wooden tower in China is currently the tallest wooden tower in the world. It was built in 1056 A.D. with a height of 65.86 m. It locates at the Yingxian county in Shanxi Province of China. The wooden tower was built of wood only without the use of any other material. In the past 956 years, the tower has experienced numerous seismic excitations, wind actions and bombardments from wars. Combined with the weakening of material, local damages of different extent could be found in some members of the structure. At present, the wooden tower inclines towards the North-East direction and the inclination increases each year.

The Yingxian wooden tower is an important cultural heritage structure in China, and many studies have been done with an effort to maintain and repair this tower. Cheng (1966) introduced this tower in details with a summary on the structural system and joints. Li *et al*. (2005) discussed the local deformation, damage, bearing capacities and reliability of the tower members. Wind load is an important and common type of loading action on this wooden tower, and is believed to relate

*Corresponding author, Associate Professor, E-mail: bochenbj@gmail.com

http://www.techno-press.org/?journal=was&subpage=8 ISSN: 1226-6116 (Print), 1598-6225 (Online)

strongly to the structural inclination over the many years of action. On site full-scale measurement is considered to be the most reliable method to collect information on the wind characteristics and the wind effects of this wooden tower. The structural modal parameters could subsequently be obtained from the field measured data.

A number of full-scale measurements on the wind effects and the modal identification of tall buildings, low-rise buildings and long-span bridges have been performed. Kwok *et al*. (1990) studied the effect of tuned mass damper (TMD) on reducing the wind-induced response of Sydney Tower with the full-scale measurement data. Tamura *et al*. (2002) and Chmielewski *et al*. (2009) showed the validity of Global Positioning System (GPS) for wind-induced response measurements of a full-scale tower. Li *et al*. (2007) and Fu *et al*. (2008) studied the wind-induced response of some typical tall buildings in China, and the amplitude-dependent damping ratios were identified by the Random Decrement Technique. Caracoglia *et al*. (2009) conducted some full-scale measurements and investigated the wind characteristics and wind pressures on roofs under hurricanes and ordinary storms. Chen *et al*. (2013) employed the wind tunnel test and full-scale measurements to investigate the effect of the surface roughness on wind loads on chimneys. John *et al*. (2003) performed full-scale long-term monitoring of wind buffeting of the Second Severn Crossing cable-stayed bridge and compared them with the results of Davenport's analytical method. The structural modal parameters could be obtained from these field measured data. Identification methods include the Peak-Picking, Frequency Domain Decomposition, Stochastic Subspace identification (SSI) method, Random Decrement Technique (RDT), wavelet analysis, and Hilbert-Huang transform (HHT) method, Huang *et al*. (1998) developed the HHT method to identify structural parameters for analyzing non-stationary data, and this method was widely used in recent years. Pines and Salvino (2006) discussed the application of HHT method in the health monitoring of structures, which was validated in a civil building model experiment. Shi *et al*. (2012) identified the modal parameters of Shanghai World Financial Center from both the free and ambient vibration with the HHT method and RDT. Roveri and Caraterra (2012) detected the damage location under traveling loads by the instantaneous frequency obtained with the HHT. The field measured fluctuating wind speed and wind-induced response are usually non-stationary, and HHT is an effective method to identify the structural modal parameters. Stochastic Subspace identification method is also widely used in civil engineering structures. Yu *et al*. (2005) combined the Empirical Mode Decomposition (EMD) and stochastic subspace identification method to identify the modal parameters of one bridge. Alicioglu *et al*. (2008) investigated the benefits and difficulties of the stochastic subspace identification method in the modal identification for several models and structures.

This paper presents the full-scale measurements of the wind velocity and the wind-induced acceleration response of Yingxian wooden tower. The characteristics of wind velocity are investigated, such as the wind direction, average wind speed, turbulence integral length scale and the velocity spectrum. Structural modal parameters of this tower are identified by two different modern modal identification methods, including the Empirical Mode Decomposition (EMD) method combined with the Random Decrement Technique (RDT) and Hilbert transform (HT), and the stochastic subspace identification method.

2. Outline of full-scale measurement system

2.1 The Yingxian wooden tower

The octagonal-shaped tower is 65.86 meters high and 30 meters in diameter at the bottom. It has five storeys when looking from outside. Each storey, except the ground storey, includes one upper story and one mezzanine story, as shown in Fig. 1(c). Each of the upper story has two rings of columns, and the outer ring of columns is connected to the inner ring of columns by beams. The mezzanine story is similar to a strengthened transfer floor of modern structures, where the outer ring of columns is connected to the inner ring of columns by trusses. Fig. 1(b) shows the typical connecting joint between the beams and columns. The outer surrounding walls from the 2nd to the 5th storey have ventilated windows, and wind can pass through the tower.

(a) Photograph of the Wooden Tower

(b) Typical structural node

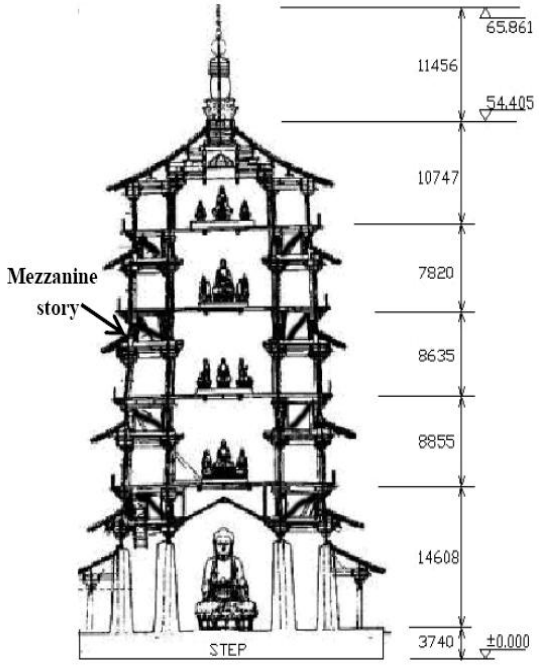

(c) Vertical section

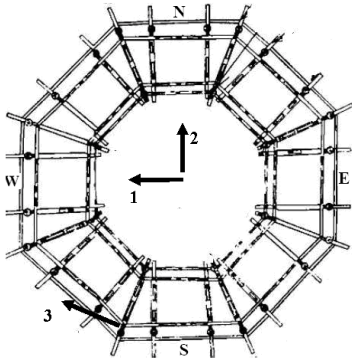

(d) Horizontal plane and accelerometers

Fig. 1 Yingxian Wooden Tower

2.2 The equipment and measuring system

The full-scale measurement system includes one ultrasonic anemometer, three accelerometers and associated data acquisition systems. An ultrasonic anemometer is installed to measure the atmospheric wind speed, to investigate the wind field and the relationship between the wind and wind-induced response of the tower. The anemometer should be placed in a relatively open position, where the atmospheric flow is unaffected by the local surrounding topography and the wooden tower itself.

Fig. 2 shows the surrounding topography around the wooden tower, which are photographed from the top floor of the wooden tower. It can be seen that the surrounding buildings are much lower than the wooden tower, while the west and north sides are relatively open. There is one large newly-constructed palace near the north side, which is about 200 m away on the tower.

The ultrasonic anemometer is installed at the top of one telecommunication tower. This telecommunication tower is a lattice steel tower, and 1000 m away from the west side of the Yingxian wooden tower. Fig. 3(a) shows the relative location of the telecommunication tower to the wooden tower. The location of the anemometer is 49.8 m high above the ground, which is almost at the same level as the top eave of the wooden tower.

(a) East (b) West

(c) South (d) North

Fig. 2 Photographs of the surrounding topography of the Wooden Tower

The R.M.Young's 3-D ultrasonic anemometer is shown in Fig. 3(b). It can measure the 3-D fluctuating wind speed and wind directions. The sampling frequency is set at 20 Hz. The wind direction is defined in degrees as shown in Fig. 4.

It is forbidden to use electricity and long vertical electric wires to prevent electrical fires and lighting in this wooden tower. In this case, it is difficult to arrange enough accelerometers at different floors at the same time, and only three accelerometers are stalled on the top floor. Two of accelerometers are installed at the center of the top floor along the east-west and north-south directions, and another is installed along the tangential direction at one of the outer columns, as shown in Fig. 1(d). These sensors are marked as sensor 1, sensor 2, and sensor 3. The angle between the directions of the sensor 1 and sensor 3 is 22.5°. The sensors are high-sensitivity piezoelectric accelerometers, capable of accurately measuring accelerations from 0.05 Hz to 500Hz, the sensitivity is 5 V/g and the resolution is better than 0.1 milli-g. The outputs of these sensors are sampled by a 24-bit data logger. The acceleration response is sampled at 1000 Hz. The frequency range of interest for this wooden tower lies much below this sampling frequency, and a re-sampling to 50 Hz of these measured data is done.

(a) Relative position of the observation tower and the wooden tower

(b) 3-D ultrasonic anemometer

Fig. 3 Pictures of the observation tower and ultrasonic anemometer

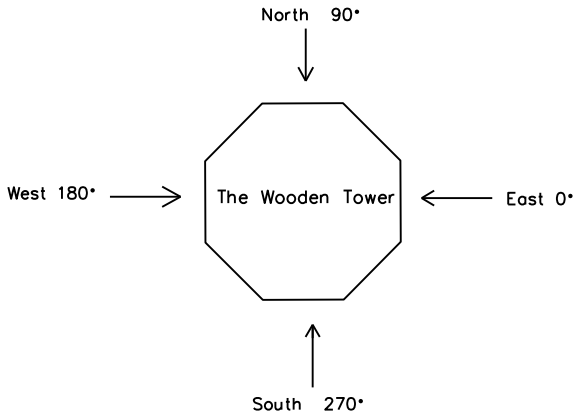

Fig. 4 Definition of the wind direction

3. Wind characteristics

Meteorological record in the Yingxian county shows that the strongest wind usually occur in November each year. Thus the full-scale measurements of the Yingxian wooden tower was conducted from Oct. 31, 2010 to Dec.15, 2010.

3.1 Wind speed and wind direction

The recorded wind data from the 3-dimensional anemometer includes three time series $u_x(t)$, $u_y(t)$ and $u_z(t)$, where the *x*, *y* and *z* denote the axis pointing to the West, the North and the vertical direction respectively. This paper defines the wind direction from the east as 0°, from the north as 90°, and from the west as 180°, which are shown in Fig. 4. The time duration for the average wind speed is 10 minutes. The 10-min average horizontal wind speed U and the average wind direction ϕ are determined from

$$U = \sqrt{\overline{u_x}^2 + \overline{u_y}^2} \tag{1}$$

$$\cos\phi = \frac{\overline{u}_x}{U} \tag{2}$$

where $\overline{u}_x$ and $\overline{u}_y$ are the mean value of time series $u_x(t)$ and $u_y(t)$ respectively.

The 10-min average vertical wind speed W is $W = \overline{u_z(t)}$.

The fluctuating longitudinal wind speed $u(t)$, the lateral fluctuating wind speed $v(t)$ and vertical fluctuating wind speed $w(t)$ can be calculated from the following equations

$$u(t) = u_x(t)\cos\phi + u_y(t)\sin\phi - U \tag{3}$$

$$v(t) = -u_x(t)\sin\phi + u_y(t)\cos\phi \tag{4}$$

$$w(t) = u_z(t) - W \tag{5}$$

Fig. 5 shows the variation of the 10-min average wind speed and wind direction with time on 26th November 2010. The maximum 10-min average wind speed reaches 14.5 m/s.

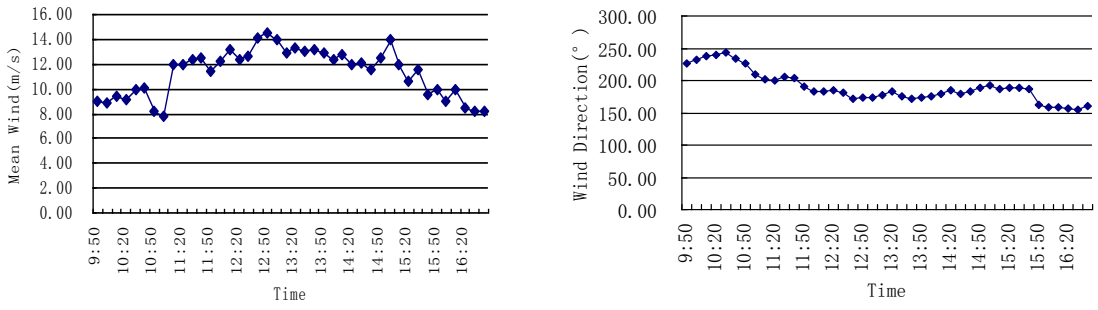

(a) 10-min average wind speed (b) 10-min average wind direction

Fig. 5 10-min average wind speed and wind direction in 11/26/2010

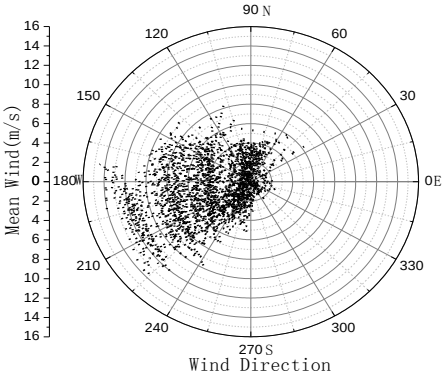

Fig. 6 10-min average wind speed and wind direction

Fig. 6 shows the 10-min average wind speed and wind direction from Oct. 31, 2010 to Dec.15, 2010. It can be seen that the strong wind is predominantly coming from the West-South direction with $150^{\circ} \le \phi \le 240^{\circ}$, and few occurs in other directions. This predominant direction is the same as the inclination of the wooden tower which is towards the North–East direction. Thirty years of statistical data of the Yingxian Meteorological Administration from propeller anemometers also show that the west is the predominant wind direction.

3.2 Turbulence intensity and gust factors

From the fluctuating wind speed and 10-min average wind speed, turbulence intensities in longitudinal, lateral and vertical directions can be determined as followed

$$I_i = \frac{\sigma_i}{U} (i = u, v, w) \tag{6}$$

where σ_u, σ_v and σ_w are the root mean square (RMS) values of the fluctuating wind speed in longitudinal, lateral and vertical direction, respectively.

Based on the field measured data, the turbulence intensities in the longitudinal, lateral and vertical directions are investigated. Fig. 7 shows the variations of the turbulence intensity in these three directions with the 10-min average wind speed. It shows that the turbulence intensity decreases with the increase of the 10-min average wind speed, and the decrease is smaller when the average wind speed is higher than 4.0 m/s. Fig. 8 gives the correlation among the turbulence intensities in longitudinal, lateral and vertical direction. It is seen that the correlations are strong especially in the range of lower turbulence intensities, where the average wind speeds are high. The correlations among these turbulence intensities are fit with the velocity samples where the average wind speed is higher than 4.0 m/s. The average ratio among these turbulence intensities is $I_u : I_v : I_w = 1 : 0.81 : 0.60$, Solari (2001) shows $I_u : I_v : I_w = 1 : 0.75 : 0.50$, and Cao *et al*. (2009) shows that the ratio is $I_u : I_v : I_w = 1.8 : 1.5 : 1.0$ of a strong typhoon (Typhoon Maemi 2003) .

Gust factors of the longitudinal wind are calculated, which is defined as the ratio between the longitudinal peak velocity within the gust duration $t_g = 3s$ to the 10-min average wind speed. Fig. 9 gives the relationship between the longitudinal gust factors with 10-min average wind speed

and the turbulence intensity. It is found that the trend of the relationship between the longitudinal gust factors with 10-min average wind speed is very similar to that in Fig. 7. Fig. 9(b) fits the samples where the average wind speed is higher than 4.0 m/s, and it shows that the gust factor is approximately linearly varying with the longitudinal turbulence intensity. A least-squares fit of the data gives the relationship $G_u(3s) = 2.19I_u + 1.0$.

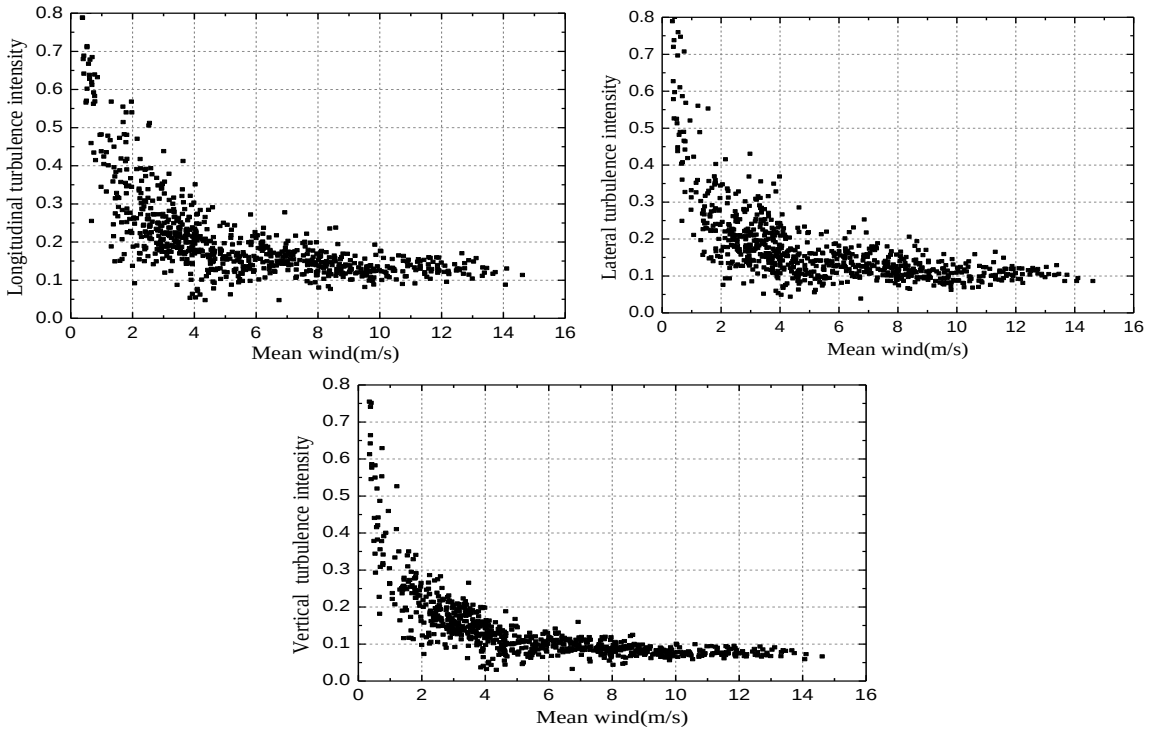

Fig. 7 Turbulence intensity in three directions

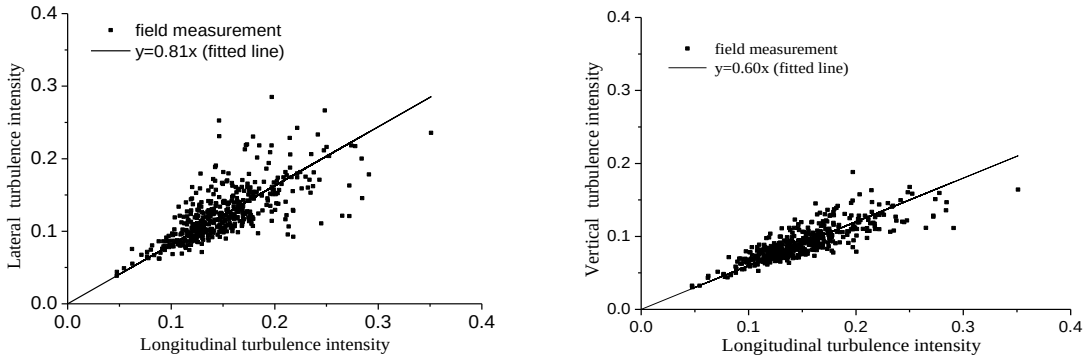

(a) 10-min average wind speed (b) 10-min average wind direction

Fig. 8 Relationship among the turbulence intensity in three directions

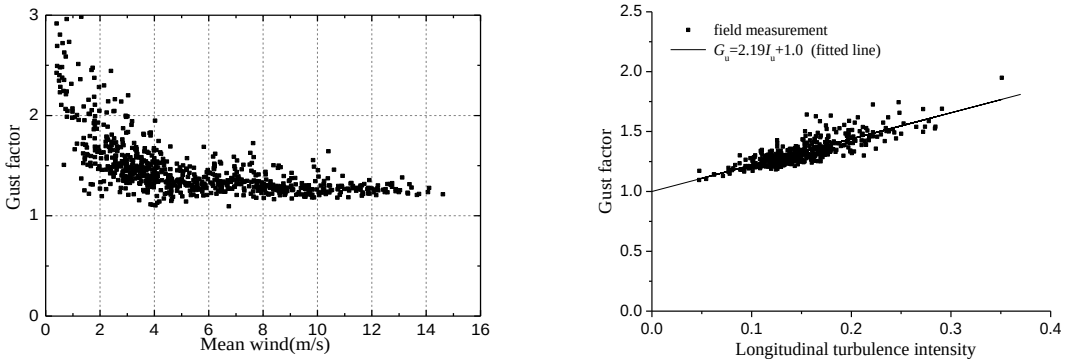

(a) Gust factor and the average wind speed (b) Gust factor and longitudinal turbulence intensity

Fig. 9 Longitudinal gust factor

The turbulence integral length scale can be estimated by the auto-correlation function with Taylor's hypothesis, or by fitting the power spectrum of the fluctuating wind speed. In general, the result obtained from the auto-correlation function is unstable and is very sensitive to the integral range of the auto-correlation function. In this paper, the Von Karman spectrum is used to fit the spectrum of the field measured wind speed to obtain the turbulence integral length scale with the least-squares fit. The Von Karman spectrum is expressed as

$$\frac{fS_u(f)}{\sigma_u^2}=\frac{4L_u f/U}{\left[1+70.8(L_u f/U)^2\right]^{5/6}} \tag{7}$$

$$\frac{fS_\varepsilon(f)}{\sigma_\varepsilon^2}=\frac{4L_\varepsilon f/U\left[1+755.2(L_\varepsilon f/U)^2\right]}{\left[1+283.2(L_\varepsilon f/U)^2\right]^{11/6}} \quad (\varepsilon=\text{v,w}) \tag{8}$$

where f is the frequency; L_u, L_v, L_w are the longitudinal, lateral and vertical turbulence integral length scale respectively; S_u, S_u, S_u are the longitudinal, lateral and vertical velocity spectrum respectively; U is the 10-min average wind velocity.

Fig. 10 shows the turbulence integral length scales from the field measured data. It is seen that the longitudinal, lateral and vertical turbulence integral length scales have weak dependency on the average wind speed. The average values of the turbulence integral length scale in these three directions are 78.0 m, 53.9 m and 19.6 m respectively with the samples where the average wind speed is higher than 4.0m/s, and the average ratio among these turbulence integral length scales is $L_u:L_v:L_w=1:0.69:0.25$. This result is close to that of Cao *et al*. (2009) where the ratio is $L_u:L_v:L_w=5.5:2.3:1.0$ of the Typhoon Maemi 2003. Fu (2008) showed that ratio is $L_u:L_v:L_w=1:0.57:0.30$ from the wind speed data measured in Shenzhen of China.

Fig. 11 compares the spectrum of the field measured wind speed to Von Karman spectrum. It can be seen that the Von Karman spectrum in Eqs. (7) and (8) can describe the spectrum of the longitudinal, lateral and vertical wind speed very well, and it indicates that it is reasonable to estimate the turbulence integral length scales by fitting the spectrum of the field measured velocity by Von Karman spectrum. Li (2007) and Cao *et al*. (2009) also show that the von-Karman spectrum is able to describe the fluctuating wind velocity.

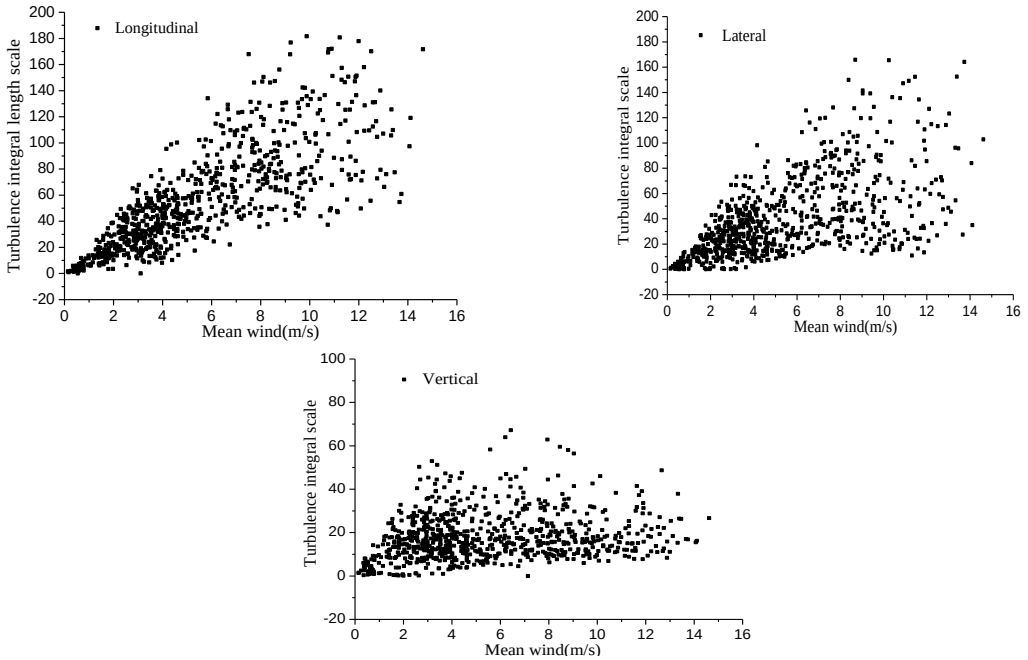

Fig. 10 Relationship between the turbulence integral length scale and 10-min average wind speed

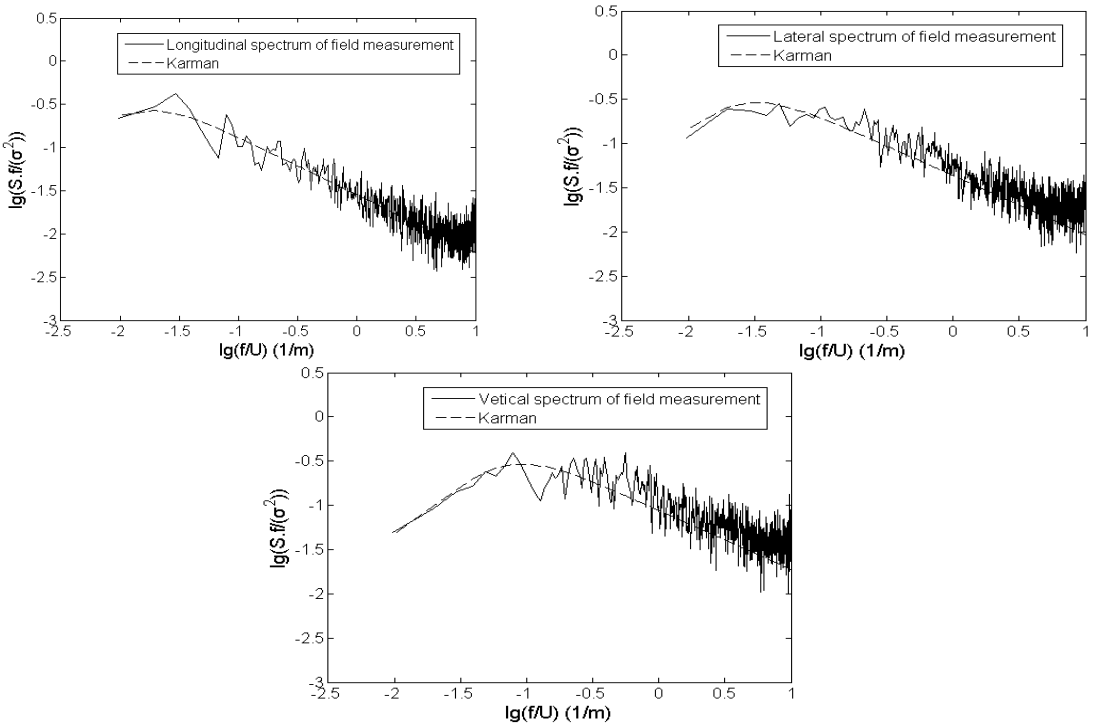

Fig. 11 Power spectral density of fluctuating wind speed

These characteristics of wind velocity around the Yingxian wooden tower are useful for future investigations on the wind loads of this wooden tower. Boundary layer simulation according to these measured wind velocity parameters in wind tunnel will be more reliable to determine the wind pressure on this tower with simultaneous pressure measurements or to measure the drag and lift wind force coefficients with high frequency force balance test.

4. Wind-induced response and structural parameters

4.1 Acceleration response

Full-scale measurements of wind-induced response were conducted on 23rd November 2010 from 16:47:10 to 17:17:09, and the temperature during this time changed from 8.1℃ to 7.2℃. The signals of all sensors are filtered by low pass filter range from 0 Hz to 15 Hz. The measured acceleration response time histories are shown in Fig. 12. The associated 10-min average wind speed and wind direction are listed in Table.1. The acceleration of sensor 3 includes the horizontal drift component which may be due to the bending mode and the torsional component which may be due to the rotation of the tower. The torsional acceleration component $a_{\omega}(t)$ in sensor 3 can be calculated as followed

$$a_{\omega}(t) = a_3(t) - (a_1(t)\cos\theta + a_2(t)\sin\theta) \tag{9}$$

where $a_1(t), a_2(t), a_3(t)$ are respectively the instantaneous acceleration of sensor 1, sensor 2 and sensor3; $\theta = 22.5°$ is the angle between the directions of sensors 1 and sensor 3.

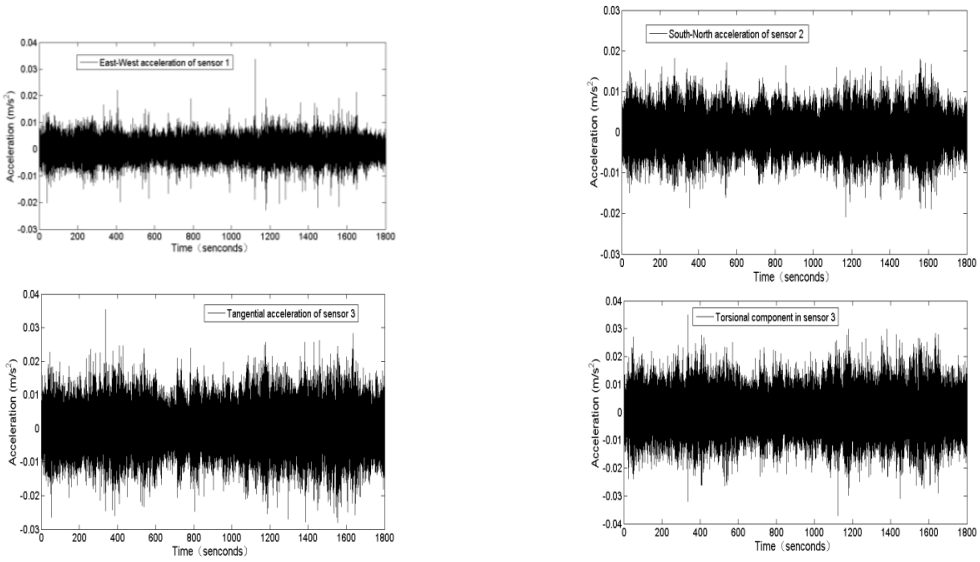

Fig. 12 Time history of the accelerations

Table 1 The average wind speed and RMS acceleration

Time	Wind		RMS of acceleration(m/s^2)			
	Average wind speed (m/s)	Wind direction (°)	Sensor 1	Sensor 2	Sensor 3	torsional component in sensor 3
16:47-16:57	7.81	204.9	0.0033	0.0037	0.0052	0.0058
16:57-17:07	7.27	200.9	0.0031	0.0033	0.0049	0.0055
17:07-17:17	8.13	208.6	0.0033	0.0038	0.0056	0.0062

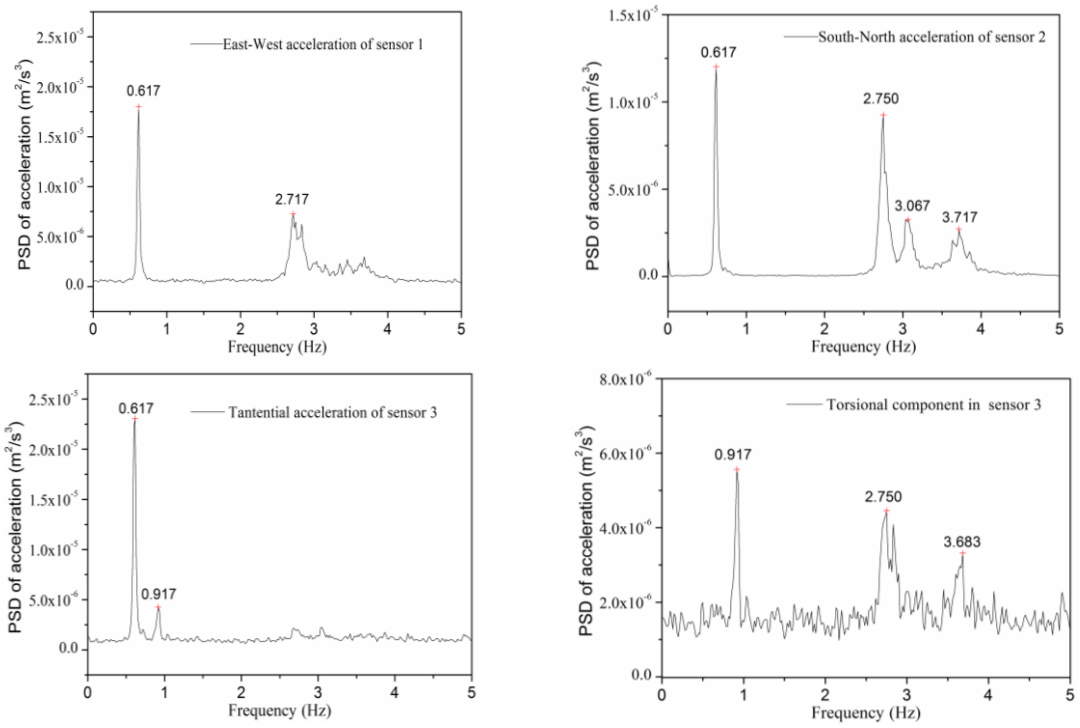

Fig. 13 PSD of the acceleration response

It can be seen from Fig. 12 and Table 1 that the wind direction is close to the west and the cross-wind response (the response of sensor 2) is close to the along-wind response (the response of sensor 1); serious torsional vibration occurs in this tower, and it is bigger than the along-wind and cross-wind response. Moreover, the correlation coefficients between the tangential acceleration and the torsional component of sensor 3, between the tangential acceleration in sensor 3 and the drift acceleration in sensor 1, between the tangential acceleration in sensor 3 and the drift

acceleration in sensor 2 are calculated, and they are 0.938, 0.053 and 0.029 respectively. This results show that the torsional vibration of the tower is the main vibration component in sensor 3, compared to the drift vibration.

Fig. 13 shows the PSDs of these three accelerations and the torsional component of sensor 3. The frequencies are obtained from the FFT analysis using maximum frequency 50 Hz and FFT size of 6144. Fluctuating wind is a broad band random process, and it had no distinct peaks in its PSD. Thus the peaks found in the PSD are the structural vibration frequencies. Peaks at 0.617 Hz occurs in the PSDs of all three accelerometers, but Peaks at 0.917 Hz occurs only in the PSD of the torsional accelerometer. It can be deduced that 0.617 Hz and 0.917 Hz are representing the frequency of one drift vibration mode and one torsional vibration mode respectively.

4.2 Structural natural frequency and damping ratio

The natural frequency and damping ratio are important to estimate the structural response under wind loads and earthquake actions, and they are necessary information to associate with the ultimate bearing capacity of this wooden tower. In this paper, two different methods are employed to identify the structural modal parameters of the Yingxian wooden tower, including the Empirical Mode Decomposition (EMD) method combined with the Random Decrement Technique (RDT) and Hilbert transform (HT), and the stochastic subspace identification method.

The main steps of the Empirical Mode Decomposition (EMD) combined with the Random Decrement Technique (RDT) and Hilbert transform (HT) are as follows:

(1) Decompose the measured data. The acceleration data are decomposed into Intrinsic Mode Functions (IMFs) with the EMD.

(2) Select useful IMFs. Peaks of the power spectral density (PSD) of these IMFs are compared with the peaks in the PSD of the structural response. If the frequency of the peaks are close together, the IMF is taken as a useful IMF.

(3) Obtain free-decay vibration response. The free-decay vibrational responses of these useful IMFs are obtained by the RDT.

(4) Identify modal parameters. Hilbert transform of these free-decay vibration responses are done to identify the structural natural frequency and damping ratio.

Details of Empirical Mode Decomposition (EMD) and Hilbert transform (HT) can be found in Huang (1998). The Random Decrement technique (RDT) and the stochastic subspace identification (SSI) method can be referred to Ibrahim (1977), Peeters (2001) and Alicioglu (2008) respectively.

Fig. 14 shows the first 10 Intrinsic Mode Functions (IMFs) of sensor 1 with EMD. The periods of these IMFs are in ascending order. Free-decay vibrations of these IMFs are obtained with the RDT. Different triggering thresholds are tried to get the fully decayed vibration response with RDT. The free-decay vibration and PSD of the 6th IMF are shown in Fig. 15, where the triggering threshold is 1.0σ and σ is the RMS of the acceleration of sensor 1. Hilbert transform is done for this free-decay vibration. PSDs of the IMFS and PSDs of free-decay vibrations of these IMFs are compared to the PSD of the structural response plotted in Fig. 13. It is found that the peak in the 6th IMF corresponds to is 0.613Hz and it is close to the peak frequency of the structural response in Fig.13. The instantaneous phase angle and amplitude are shown in Fig. 16. The frequency and damping ratio are obtained with least-squares fit, and they are 0.619 Hz and 2.29% respectively. It can be seen that the fitted phase and amplitude are both very close to the measured values.

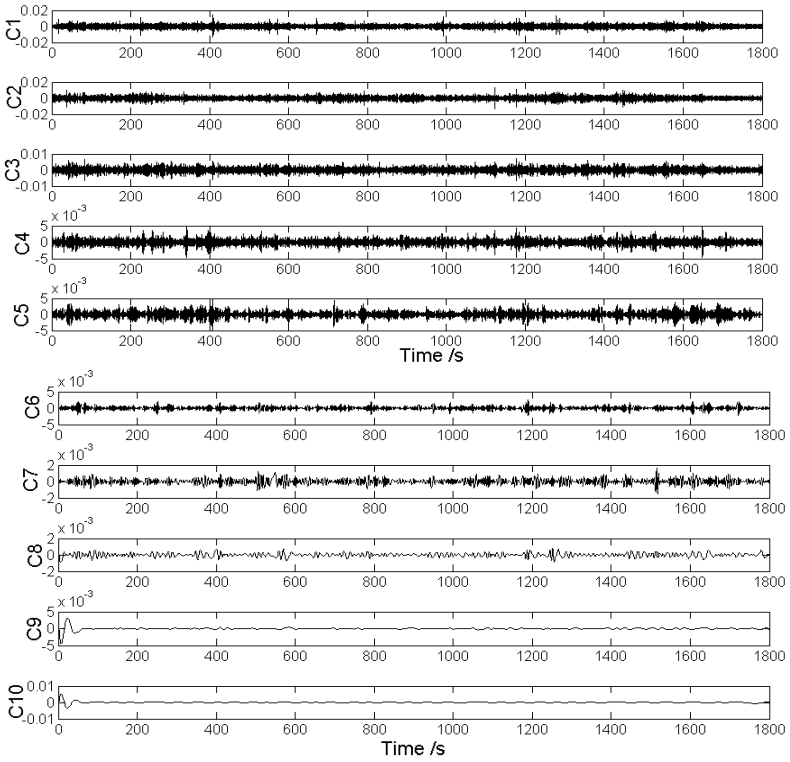

Fig. 14 IMFs of the vibration acceleration of sensor 1 by EMD

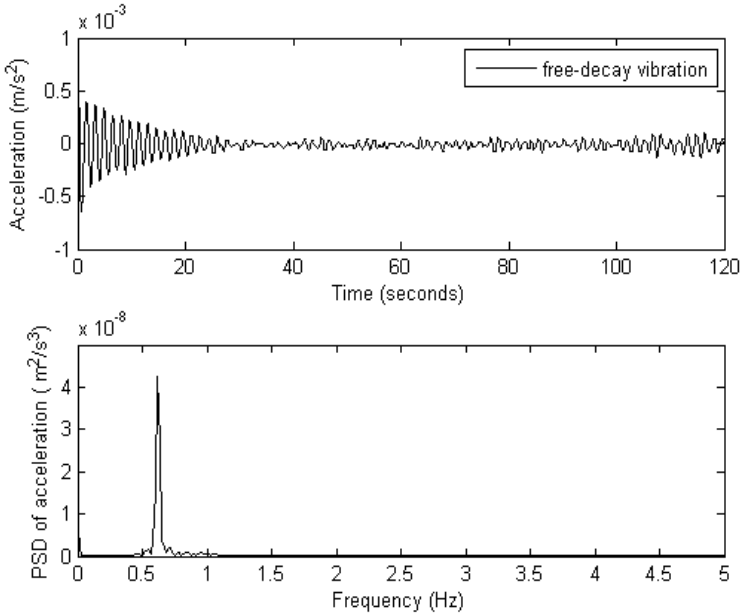

Fig. 15 Free-decay vibration of the 5th intrinsic mode for sensor 1 by RDT

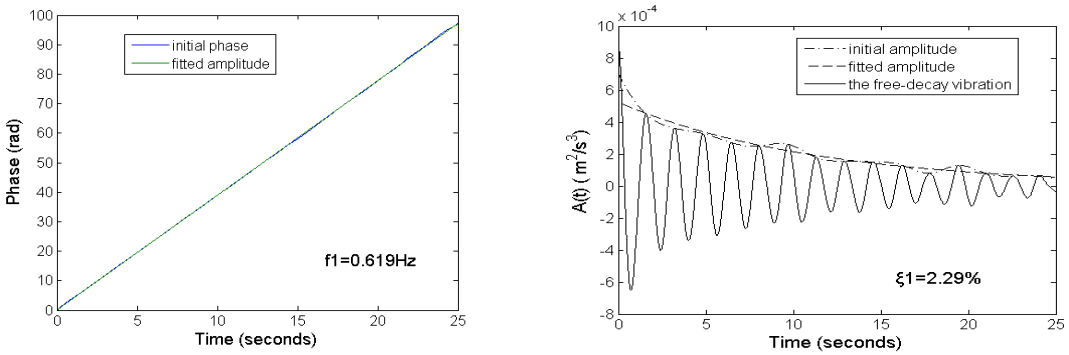

Fig. 16 Modal parameters of the 5th intrinsic mode for sensor 1

The RDT and Hilbert transform are performed for the other first 5 IMFs of the acceleration in sensor 1, but only the PSD of the 4th IMF has obvious peak, where the triggering threshold is 1.2 σ. The corresponding identified natural frequency and damping ratio are 2.705Hz and 3.76% respectively.

The identification analysis from the response of sensor 2 and sensor 3 is also similarly performed. The instantaneous phase angle and amplitude of the free-decay vibration of the 6th IMF in sensor 2 are shown in Fig. 17, and the adopted triggering threshold in RDT is 0.95 σ to obtain their free-decay vibrations. It is seen from Fig. 13 that the peak at 0.917 Hz of the torsional component is weaker than the peaks at 0.617 Hz of one drift vibration component. It is difficult to directly identify the torsional frequency and damping ratio from the response in sensor 3 or the torsional component in sensor 3. Thus, the signal of the torsional component in sensor 3 is filtered by band pass filter from 0.8 Hz to 1.0 Hz before the RDT and Hilbert transform. The instantaneous phase angle and amplitude are shown in Fig.18, and the triggering threshold adopted is 1.3 σ to obtain their free-decay vibrations. The identified natural frequency and damping ratio are 0.929 Hz and 3.16% respectively.

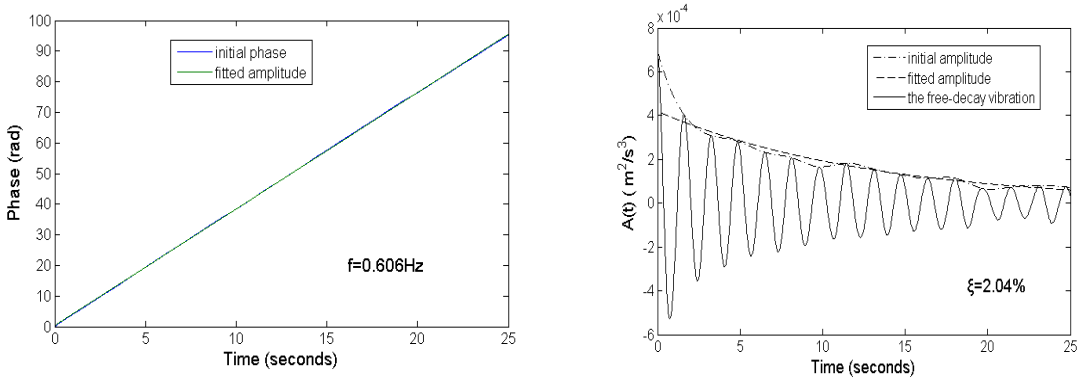

Fig. 17 Modal parameters of the 6th intrinsic mode for sensor 2

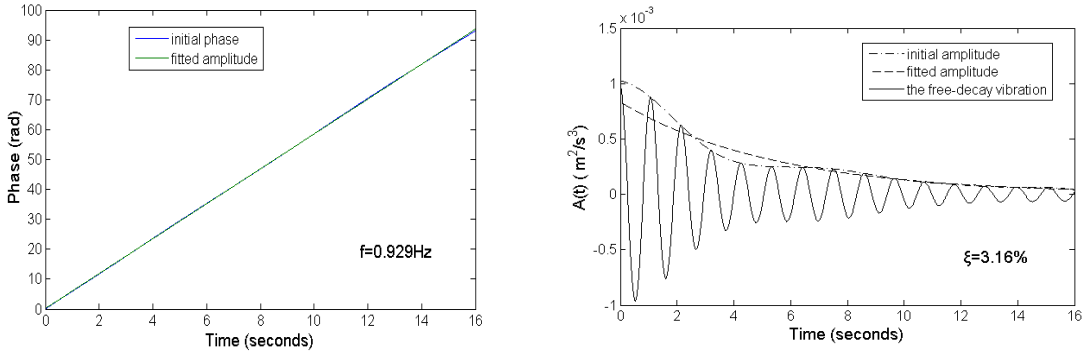

Fig. 18 Modal parameters of the 1th intrinsic mode for the torsional component in sensor 3

In order to obtain the free-decay vibration by the RDT, the triggering threshold determines the superimposition number of response segments from the dynamic response. Therefore, it affects the identified modal parameters. Table 2 shows the effects of the superposition number on the identified frequency and damping ratio from the 5th intrinsic mode for sensor 1. It can be seen that the superimposition number has more important effects on the damping ratio than the frequency, and the identified modal parameters deviate much from the mean value when the superimposition number is too small or big. On the basis of this result, the mean values of identified modal parameters when the superimposition number makes the identified values stable are chosen to represent the structural modal parameters. For the 5th intrinsic mode for sensor 1, the mean values of the identified frequency and damping ratio when the superimpostition number ranges from 488 to 1092 are 0.618Hz and 2.31% respectively. The effects of the superimposition number in the RDT are also investigated for all other intrinsic modes of sensor 1, sensor 2 and sensor 3. The mean values of the identified modal parameters obtained from different superimposition numbers in the RDT are listed in Table 3.

Table 2 Effects of the superimposition number in the RDT on modal parameters for sensor 1

triggering threshold	number of superimposition	frequency(Hz)	damping ratio(%)
1.60σ	360	0.616	1.85
1.40σ	488	0.617	2.14
1.25σ	620	0.619	2.41
1.10σ	774	0.618	2.47
1.00σ	922	0.619	2.29
0.80σ	1092	0.618	2.24
0.60σ	1294	0.617	1.94

The stabilization diagram is usually used to determine the reliable modal parameters in the stochastic subspace identification method. A stabilization diagram is a plot of various model orders versus identified natural frequencies at each model order, where an actual identified system mode

should show consistent frequency at various model orders, but those in the spurious identified system modes will be erratic. Fig. 19 shows the stabilization diagram of the Yingxian wooden tower. It can be seen that the frequency around 0.61 Hz, 0.93 Hz, 2.70 Hz and 3.0 Hz is stable for those model orders, around n>80, and these frequencies can be regarded as the real natural frequencies of the Yinxian wooden tower. Damping ratios corresponding to these frequencies are also obtained. The identified modal parameters are shown in Table 3. The frequencies and damping ratios listed in this table are the mean values for various model orders, n>80.

The identified structural modal parameters of Yingxian wooden tower by using the EMD, RDT and Hilbert Transform are compared to those by using the stochastic subspace identification method. It can be seen that the natural frequencies of each mode identified by these two methods are very close to each other, but the damping ratios for the first two modes by EMD, RDT and Hilbert Transform are bigger than those by the stochastic subspace identification method.

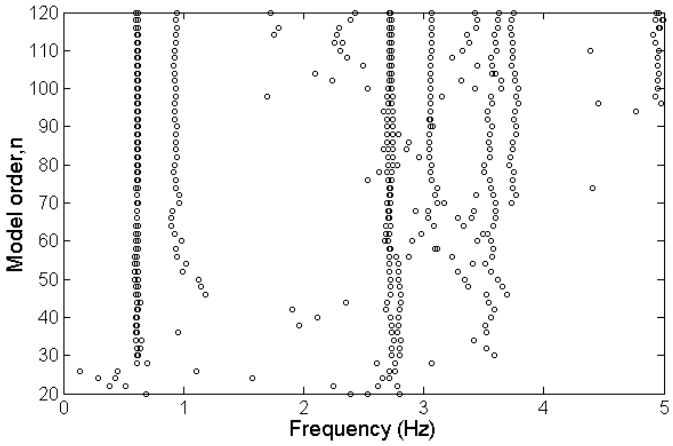

Fig. 19 Stabilization diagram of the identified frequencies for various model orders by the SSI method

Table 3 Identified structural modal parameters

	EMD+RDT+HT		SSI	
Mode	frequency(Hz)	damping ratio(%)	frequency(Hz)	damping ratio(%)
1st	0.607	2.34	0.609	1.47
2nd	0.618	2.31	0.620	1.70
3rd	0.931	3.38	0.933	2.97
4th	2.692	3.78	2.707	3.33
5th	2.740	1.73	2.735	1.87
6th			3.057	1.06

5. Conclusions

This paper presented the full-scale measurements of wind effects and modal parameter identificaiton of the Yingxian Wooden tower. Wind characteristics of the average wind speed, wind direction, turbulence intensity, gust factor, turbulence integral length scale and velocity spectrum

are investigated. Structural modal parameters of this tower are identified by two methods, including the Empirical Mode Decomposition (EMD) combined with the Random Decrement Technique (RDT) and Hilbert transform (HT), and the stochastic subspace identification method. Some conclusions are drawn as follows:

- The wind speed has the tendency that the turbulence intensities and gust factors of the longitudinal, lateral and vertical wind speed become smaller with the increasing of the average wind speed. The ratio among these turbulence intensities is $I_u : I_v : I_w = 1 : 0.81 : 0.60$. The gust factor is about linear to the longitudinal turbulence intensity with the relationship $G_u(3s) = 2.19 I_u + 1.0$.
- The Von Karman spectrum can describe the spectrum of the longitudinal, lateral and vertical wind speed well. The ratio among the longitudinal, lateral and vertical integral length scales is $L_u : L_v : L_w = 1 : 0.69 : 0.25$.
- The method is effective that combining the Empirical Mode Decomposition (EMD), the Random Decrement Technique (RDT) and Hilbert transform (HT) to identify structural parameters of this tower, where useful IMFs of the dynamic response with EMD are chosen by comparing the peak frequency of the PSD of each IMF to that of the PSD of structural dynamic response.
- The natural frequencies of the first two drift modes identified by EMD, RDT and Hilbert Transform are 0.607 Hz and 0.618 Hz respectively, and the corresponding damping ratios are 2.34% and 2.31% respectively; The natural frequency and damping ratio of the first torsional mode are 0.931Hz and 3.38% respectively.
- The natural frequency of each mode identified by these two different identification methods is very close to each other, but the damping ratios for the first two modes identified by EMD, RDT and Hilbert Transform are bigger than those by the stochastic subspace identification method.

Acknowledgments

The work described in this paper was partially supported by the National Natural Science Foundation of China (Grant No. 91215302), the Natural Science Foundation of Beijing, China (Grant No. 8112023), and the Fundamental Research Funds for the Central Universities in China (Grand No.2010JBZ011). The authors are also grateful to Professor Siu-Seong Law in the Hong Kong Polytechnic University for his good suggestions.

References

Alicioglu, B. and Lus, H. (2008), "Ambient vibration analysis with subspace methods and automated mode selection: case studies", *J. Struct. Eng. - ASCE*, **134**, 1016-1029.

Cao S., Tamura, Y., Kikuchi, N., Saito, M., Nakayama, I. and Matsuzaki, Y. (2009), "Wind characteristics of a strong typhoon", *J. Wind Eng. Ind. Aerod.*, **97**(1), 11-21.

Caracoglia, L. and Nicholas P.J. (2009), "Analysis of full-scale wind and pressure measurements on a low-rise building", *J. Wind Eng. Ind. Aerod*., **97**, 157-173.

Chen, C.H., Chang, C.H. and Lin, Y.Y. (2013), "The influence of model surface roughness on wind loads of the RC chimney by comparing the full-scale measurements and wind tunnel simulations", *Wind Struct*., **16**(2), 137-156.

Cheng, M. (1966), *Yingxian wooden tower*, Cultural Relic Press, Beijing , China.

Chmielewski, T., Breuer, P., Gorski, P. and Konopka, E. (2009), "Monitoring of tall slender structures by GPS measurements", *Wind Struct.*, **12**(5), 401-412.
Fu, J.Y., Li, Q.S., Wu, J.R, Xiao, Y.Q. and Song, L.L. (2008), "Field measurements of boundary layer wind characteristics and wind-induced responses of super-tall buildings", *J. Wind Eng. Ind. Aerod.*, **96**, 1332-1358.
Huang, N.E., Shen Z., Long S.R., Wu, M.C., Shih, H.H., Zheng, Q., Yen, N.C., Tung, C.C. and Liu, H.H. (1998), "The empirical mode decomposition and the Hilbert spectrum for nonlinear and non-stationary time series analysis", *P. Roy. Soc. Lond. A. Math. Phys. Eng. Sci.*, **454**(1971), 903-995.
Ibrahim, S.R. (1977), "Random decrement technique for modal identification of structure", *J. Spacecraft Rockets*, **14**(11), 696-700.
John H.G.M. (2003), "Evaluation of buffeting predictions of a cable-stayed bridge from full-scale measurements", *J. Wind Eng. Ind. Aerod.*, **91**(12-15), 1465-1483.
Kwok, K.C.S. and Macdonald, P.A. (1990), "Full-scale measurements of wind-induced acceleration response of Sydney Tower", *Eng. Struct.*, **12**, 153-162.
Li, Q.S., Xiao, Y.Q., Fu, J.Y. and Li, Z.N. (2007), "Full-scale measurements of wind effects on the Jin Mao building", *J. Wind Eng. Ind. Aerod.*, **95**, 445-466.
Li, T., Wei, J. and Zhang, S. *et al*. (2005), "Appraisal on the structure on the Yingxian wooden tower", *China Civil Eng. J.*, **38**(2), 51-58 (in Chinese).
Peeters, B. and De Roeck, G. (2001), "Stochastic system identification for operational modal analysis: A review", *J. Dyn. Syst. Meas. Control*, **123**(4), 659-667.
Pines, D. and Salvino, L. (2006), "Structural health monitoring using empirical mode decomposition and the Hilbert phase", *J. Sound Vib.*, **294**(1-2),97-124
Roveri, N. and Carcaterra, A. (2012), "Damage detection in structures under traveling loads by Hilbert–Huang transform", *Mech. Syst. Signal Pr.*, **28**,128-144.
Shi, W., Shan, J. and Lu, X. (2012), "Modal identification of Shanghai World Financial Center both from free and ambient vibration response", *Eng. Struct.*, **3**, 14-26.
Solari, G. and Piccardo, G. (2001), "Probabilistic 3-D turbulence for gust buffeting of structures", *Probabilist. Eng. Mech.*, **16**(1), 73-86.
Stathopoulos, T., Baskaran, A. and Goh, P.A. (1990), "Full-scale measurements of wind pressures on flat roof corners", *J. Wind Eng. Ind. Aerod.*, **36**(1-3) ,1063-1071.
Tamura, Y., Matsui, M., Pagnini, L.C., Ishibashi, R. and Yoshida, A. (2002), "Measurement of wind-induced response of buildings using RTK-GPS", *J. Wind Eng. Ind. Aerod.*, **90**(12-15), 1783-1793.
Yu D.J. and Ren, W.X. (2005), "EMD-based stochastic subspace identification of structures from operational vibration measurements", *Eng. Struct.*, **27**(12), 1741-1751.

CC